Deutsches Institut
für Kautschuktechnologie e.V.

DIK Preprints

Current topics from Rubber Technology

Manuscript intended for submission
to conference proceedings

Preprint:	2
Date:	14th March 2019
Authors:	Alexander Ricker, Nils Hendrik Kröger, Marvin Ludwig, Ralf Landgraf, Jörn Ihlemann
Title:	Validation of a hyperelastic modelling approach for cellular rubber
Cited as:	submitted to Constitutive Models for Rubber XI. Proceedings of the 11th European Conference on Constitutive Models for Rubber (ECCMR 2019, Nantes, France, 25-27 June 2019)

Validation of a hyperelastic modelling approach for cellular rubber

A. Ricker & N. H. Kröger
Simulation and Continuum Mechanics
Deutsches Institut für Kautschuktechnologie e.V., Hanover, Germany

M. Ludwig
Toyoda Gosei Meteor GmbH, Bockenem, Germany

R. Landgraf & J. Ihlemann
Chair of Solid Mechanics
Chemnitz University of Technology, Chemnitz, Germany

ABSTRACT: Cellular rubbers are elastomeric materials containing pores which can undergo large volumetric deformations. This contribution presents an isotropic, hyperelastic material model for cellular rubbers based on the approach of Danielsson, Parks, & Boyce (2004). For model validation and parameter fitting, experimental characterization were carried out for a foamed elastomers based on a natural rubber compound. Moreover, a feasible procedure of parameter fitting avoiding lateral strain measurement is outlined and tested. Furthermore, a finite element model of the microstructure of the cellular rubber is reconstructed from a computer tomography scan.

1 INTRODUCTION

Rubber products containing gas-filled cells or hollow receptacles are called cellular rubber. These two-phase materials provide a lightweight design, low reaction forces and the ability to undergo large volumetric deformations. Thus, they are widely-used for instance in seals and weather stripping applications. In order to simulate the mechanical behaviour of cellular materials, there are in general two approaches. On the one hand, one can consider the actual geometry of the microstructure and model both phases separately. This micromechanical approach is very intuitive and gives an insight to the local deformation but results in huge computational costs. It is discussed in Section 5.

On the other hand, the microstructure can also be homogenized. This approach leads to continuous material properties represented by a single material model. In this case, only the enveloping geometry of the cellular product has to be considered, but a higher modelling effort is required to predict a realistic behaviour. This approach is referred to as macromechanical and is outlined in Section 4. The presented results are based on Ricker (2018).

Various approaches have been made in order to model foamed elastomers, cf. e.g. Blatz & Ko (1962), Hill (1978), Ogden (1972), Diebels (2000), Jemiolo & Turteltaub (2000), Danielsson, Parks, & Boyce (2004), Koprowski-Theiß (2011), Lewis & Rangaswamy (2012), Wang, Hu, & Zhao (2017), Matsuda, Oketani, Kimura, & Nomoto (2017) and many more.

2 CLASSIFICATIONS OF CELLULAR RUBBER AND ITS MICROSTRUCTURE

The ASTM Committee E02 on Terminology (2005) distinguishes between three different types of cellular rubber based on the production method and cell type:

Latex foam rubber is made by stirring mechanically gas into a liquid latex compound before it is subsequently cured. Alternatively, a blowing agent can be incorporated into a solid rubber compound that decomposes during the vulcanization process and chemically produces gas bubbles. These materials are either referred to as sponge rubber in case of predominately open, interconnected cells or as expanded rubber in case of predominately closed, non-interconnected cells. This contribution focuses on the latter one.

Furthermore, additional parameters are required to

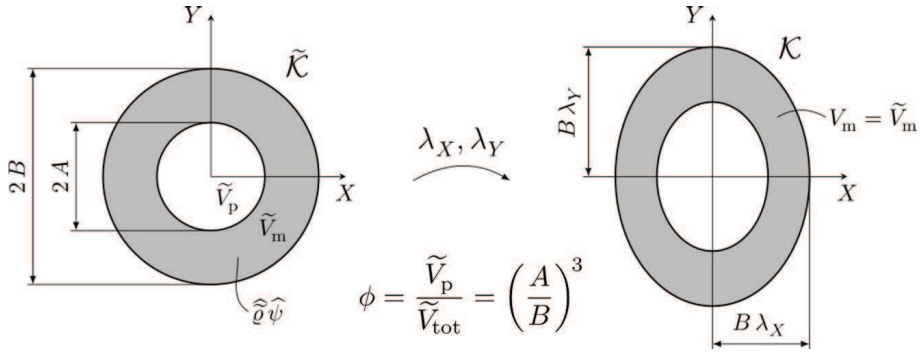

Figure 1: Representation of the volume constant deformation of a hollow sphere ($\tilde{\mathcal{K}}$ to $\mathcal{K}$) with incompressible matrix material by macromechanical stretches λ_X and λ_Y

describe the microstructure of cellular materials, for example the pore distribution, the average pore size, the pore ellipticity and many more. Here, only one parameter, the porosity, is considered:

The porosity is defined as the ratio of pore volume $\tilde{V}_p$ to the total volume of the cellular material $\tilde{V}$

$$\phi = \frac{\tilde{V}_p}{\tilde{V}_p + \tilde{V}_m} \tag{1}$$

where V_m is the volume of the matrix material. The tildes denote quantities in the undeformed, reference state. An alternative formulation can be given via the mass densities of the foam $\tilde{\rho}_f$ and pure matrix material $\tilde{\rho}_m$. Assuming the mass density of the pore fluid $\tilde{\rho}_p$ is much smaller compared to the matrix density the porosity can be approximated by

$$\phi \approx 1 - \frac{\tilde{\rho}_f}{\tilde{\rho}_m} \qquad \text{if} \qquad \tilde{\rho}_m \gg \tilde{\rho}_p. \tag{2}$$

3 MACROMECHANICAL MATERIAL MODEL

The common approach to model rubber-like materials is based on a split of the deformation into an isochoric and a volumetric part as proposed by Flory (1961). This leads to non-physical behaviour in case of highly compressible materials as shown by Ehlers & Eipper (1998). Therefore, more complex material models with coupled isochoric-volumetric properties have been developed. For example Hill (1978) presented a phenomenological strain energy function in terms of principal stretches for foamed rubber based on the works of Blatz & Ko (1962) and Ogden (1972). This hyperelastic model is implemented in many commercial finite element programs. In contrast, Danielsson, Parks, & Boyce (2004) derived a strain energy function in terms of the principal invariants of the left Cauchy-Green tensor from the kinematics of an idealized microstructure. This idea is the basis for the material model used within this contribution. The basic assumption of Danielsson et al. is that every material point within the cellular material behaves like a hollow sphere with perfectly incompressible outer layer representing a single pore. The ratio of the inner diameter A to the outer diameter B is defined by the porosity $\phi = (A/B)^3$. The behaviour of the matrix material is defined by the hyperelastic strain energy function

$$\hat{\tilde{\rho}}\hat{\psi} = \hat{\tilde{\rho}}\hat{\psi}(\hat{I}_1, \hat{I}_2) \tag{3}$$

in dependency of the local principle invariants $\hat{I}_1$ and $\hat{I}_2$. The superscript $\hat{}$ denotes the micromechanical quantities. $\hat{I}_1$ and $\hat{I}_2$ can be derived with respect to the macroscopic principal stretches λ_A and an admissible radial deformation field x_A for details we refer to Danielsson, Parks, & Boyce (2004). Under an external load the hollow sphere deforms to a hollow ellipsoid where the semi-axes are defined by the macroscopic principal stretches λ_A. Considering an admissible radial deformation field x_A on the hollow sphere the micromechanical kinematics are uniquely defined in terms of the macromechanical stretches, see Fig. 1. In order to obtain a macromechanical material model from this micromechanical kinematics, a local strain energy density is assigned to the hollow sphere. Integrating the local strain energy density, Eq. (3), of the micromechanical kinematics over the sphere volume yields the total strain energy applied on the sphere. Hence, an average, homogenized strain energy function is obtained by

$$\tilde{\rho}\psi(I_1, I_2, J, \phi, ...) = \frac{1}{\tilde{V}} \int_{G_m} \hat{\tilde{\rho}}\hat{\psi}\left(\hat{I}_1, \hat{I}_2, ...\right) \mathrm{d}\tilde{V}. \tag{4}$$

Danielsson et al. demonstrated the procedure using the Neo-Hooke local strain energy function, which leads to a compressible Neo-Hooke model. Without difficulties the approach can be extended to a compressible Mooney-Rivlin and yields

$$\tilde{\rho}\psi = (c_{10}\,(\alpha_1 I_1 - 3 + c_{01}(\alpha_2 I_2 - 3)) \cdot (1 - \phi) \tag{5}$$

as macroscopic strain energy function with

$$\alpha_1 = 2 - \frac{1}{J} - \frac{\phi + 2(J-1)}{(1 + (J-1)/\phi)^{1/3} J^{2/3}} \tag{6}$$

and

$$\alpha_2 = -1 + \frac{2}{J} - \left(\frac{J - 1 + \phi}{J\phi}\right)^{1/3} \left(\frac{\phi + 1}{J} - 1\right). \tag{7}$$

The correctness of this formula can be proven by applying porosity $\phi = 0$ and $J = 1$ which recovers the incompressible Mooney-Rivlin strain energy function. A similar approach was derived by Lewis & Rangaswamy (2012). However, Lewis & Rangaswamy (2012) applied the approach only to the isochoric part of the model where $J = 1$ and subsequently $\alpha_1 = \alpha_2 = 1$. In this case, the compressible properties finally get lost.
In case of more general local strain energy functions with higher order terms, e.g. Yeoh-model, the integral Eq. (4) cannot be solved analytically anymore. In this work the local strain energy function proposed by James, Green, & Simpson G. M. (1975) is used:

$$\begin{aligned}\hat{\tilde{\rho}}\hat{\psi} =& c_{10}\left(\hat{I}_1 - 3\right) + c_{01}\left(\hat{I}_2 - 3\right) \\ &+ c_{20}\left(\hat{I}_1 - 3\right)^2 + c_{30}\left(\hat{I}_1 - 3\right)^3 \\ &+ c_{11}\left(\hat{I}_1 - 3\right)\cdot\left(\hat{I}_2 - 3\right).\end{aligned} \tag{8}$$

Thus, numerical integration methods have to be used. To minimize the numerical effort, the integration scheme is applied to the stresses as proposed by Danielsson:

$$\tilde{\mathbf{T}} = \frac{2}{\tilde{V}} \cdot \frac{\partial}{\partial \mathbf{C}} \int_{G_m} \frac{\partial \hat{\tilde{\rho}}\hat{\phi}}{\partial \mathbf{C}} \, \mathrm{d}\tilde{V}. \tag{9}$$

The integral is split into a radial and a spherical part. The radial part is treated by a Gauss-Legendre quadrature with four integration points. Whereas, the spherical part is computed by a Lebedev quadrature, see Lebedev (1976), or uniform distributed integration points given by the vertices of the platonic solids. The distribution of integration points can be selected with symmetry in all three coordinate planes in an appropriate coordinate system. In order to prove the accuracy of the spherical integration schemes, the dependence of the quadrature result on the position of integration points can be investigated, see Ricker (2018). The coordinate system of the integration points is rotated relatively to the co-ordinate system of the sphere. Consequently, a Lebedev integration scheme with 26 integration points should be used. Since the symmetry to the coordinate planes applies to the deformation of a sphere to an ellipsoid, too, the coordinate systems are chosen to coincide. This leads to seven effective integration points. In conjunction with four radial points, 28 overall integration points have to be evaluated. The resulting material model is exemplified in Fig. 2 showing the stress response and the lateral strain in case of uniaxial tension with varying porosities.

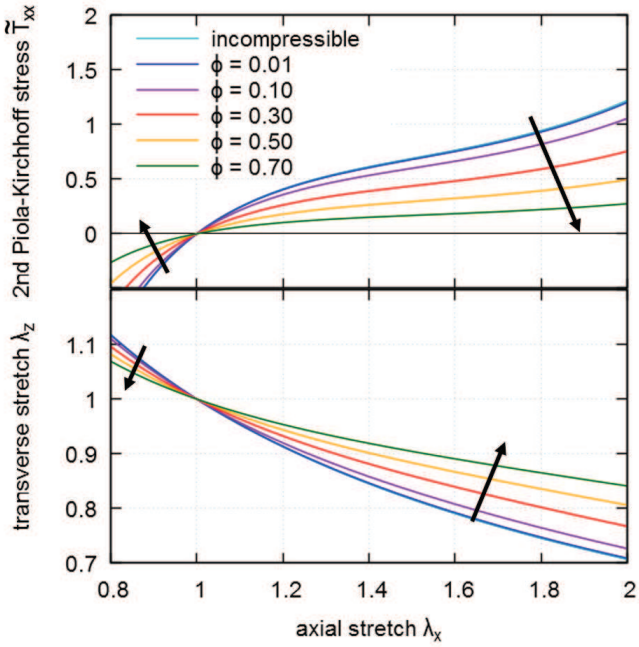

Figure 2: Material model response for varying porosity ϕ

4 EXPERIMENTS AND PARAMETER FITTING

There are some experimental challenges concerning the characterization of the mechanical properties of cellular rubber. For instance, the cellular structure tends to tear at the clamps particularly with regard to biaxial and planar tension tests. Furthermore, a testing machine with lateral strain measurements is required since the lateral stretches cannot be derived from the incompressibility constraint as usually done for pore-free rubber. Otherwise, the deformation is not entirely captured leading to unknown independent variables within the parameter fitting procedure. Therefore, a step-wise parameter fitting procedure is presented.
The basic idea of the proposed parameter fitting procedure is the fact that the aforementioned material model is derived from the kinematics of an idealized pore. Here, an incompressible strain energy function is assigned to the matrix material independently of the actual pore size. In other words, the porosity is just a geometrical quantity that does not influence the remaining material parameters c_{ij} of the strain energy function. Therefore, one can produce pore-free test specimen, fit the parameters c_{ij} assuming incompressibility and porosity $\phi = 0$ and finally add the porosity to obtain a full set of parameters for the porous material. Thus, no mechanical tests on the cellular material are needed. The outlined procedure is illustrated in Fig. 3 using a carbon black filled, sulphur cured natural rubber. The resulting parameters [in MPa] are $c_{10} = 0.3967$, $c_{01} = 0.0768$, $c_{11} = 0.0041$, $c_{20} = 0$ and $c_{30} = 0.0204$. The porosity $\phi = 0.465$ is determined by density measurements of the pore-free material and the foam material.

In order to evaluate the applicability of the material model and the parameter fitting procedure, a

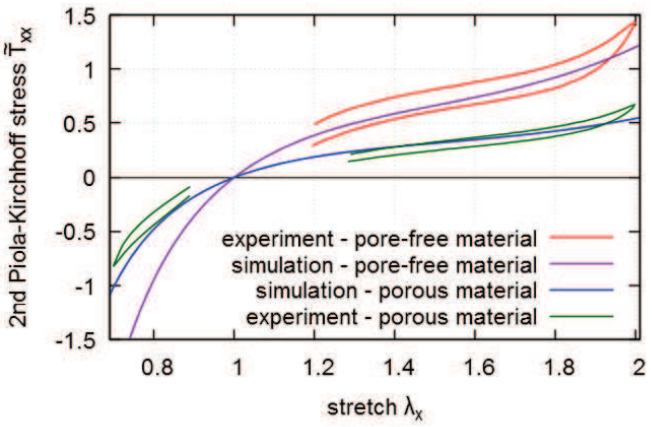

Figure 3: Resulting parameter fit for an uniaxial tension test of pore-free material and corresponding validation test for uniaxial tension and compression of the foamed elastomer. The stabilized (5th) cycles of a multi-hysteresis tests are used for identification and validation. Inelastic effects are neglected by cutting the material response at low strains.

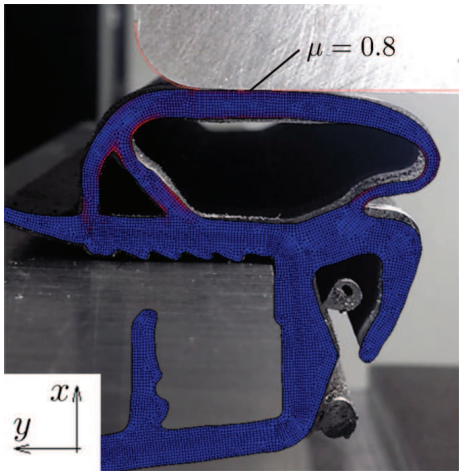

Figure 4: Comparison of compression test of a car door sealing and FEM results

compression test is carried out on a car door seal, see Fig. 4. This test measures the vertical displacement of the piston versus the vertical reaction force and is used to investigate the closing behaviour of the car door. The experiment is simulated using the FE-software MSC.Marc. The results are shown in Figs. 4 and 5. Therein, the predicted deformation is compared to a photography of the deformed seal showing a good agreement. The experimental and simulated force vs. displacement curves show rather good agreement as well. Especially, since the pore distribution and inelastic effects are not yet accounted for. For instance, due to production processes the outer hull of the seal contains less pores, such that adjustments have to be made in setting up the FE model with varying porosities.

5 MICROMECHANICAL SIMULATIONS

Instead of a macromechanical modelling approach, see Section 3, a direct modelling via the geometry of the foamed elastomer can be chosen as well. Due to numerical limitations only small volumes can be

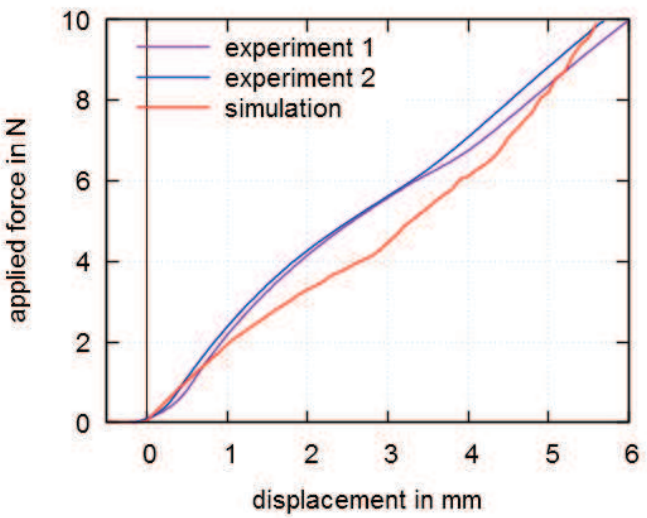

Figure 5: Comparison of force vs. displacement of test and simulation results of a compressed car door sealing

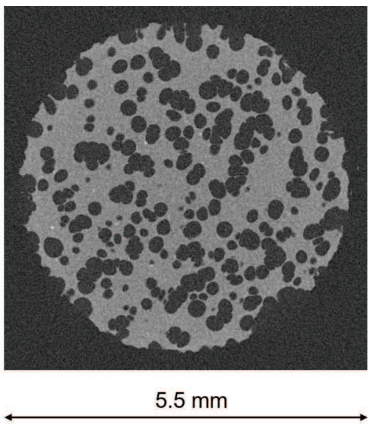

Figure 6: Computed tomographic layer of a cylindrical specimen of the foamed material (natural rubber): The recording consists of 600 vx $\times$ 600 vx and captures one section of 5.5 mm $\times$ 5.5 mm

considered. Via computer tomography (CT) measurement the pore structure is analysed for a cylindrical probe, see Fig. 6. A 0.9 x 0.9 mm cube of the geometry is reconstructed from the 2D images using the Software MeVisLab (Version 3.0.1) and imported in MSC.Marc. Due to image noise and the blurred transitions between phases clear boundaries cannot be found without difficulties. The final geometry output therefore depends on the segmentation algorithm as well as the pre- and post-processing of the CT images. For this work, the segmentation parameters are chosen such that the ratio from the segmented volume to the total volume of the cube is approximately $1 - \phi$. A fully representative sub-cell of the foam can not be easily identified due to the inhomogeneous pore distribution in the probe. For illustrative purposes, only one sub-cell is modelled and investigated.

Using the parameters for the pore-free material as (quasi-)incompressible matrix material, see Section4, an uniaxial tension test is simulated, see Fig. 7.

In MSC.Marc incompressible materials are modelled quasi-incompressible. The strain energy func-

tion is extended by a volumetric part

$$\tilde{\psi}_{vol} = \frac{9}{2} K \left(J^{1/3} - 1 \right)^2 . \tag{10}$$

The bulk modulus K is set to 20GPa and a Hermann element formulation is used (MSC Software Corporation 2017). As element type linear 4-node or 10-node elements can be used. Deciding on one of the element types is a trade-off between the computational effort, the local accuracy and stability. The use of 4-node tetrahedral elements leads to similar stress-strain responses as the 10-node elements, and reduces the number of nodes from 401216 to 58740. Due to high deformations within the foam structure the application of the 10-node element type leads to numerical instabilities, too. Therefore, for the presented investigations only 4-node linear elements are used.

The boundary conditions can be set in different variants, especially for the sides of the cube, e.g. free deformable, symmetrical or periodical. Here, an alternative is used. The boundary conditions are chosen such that the enveloping geometry of the material section always remains a cube with flat side surfaces. This means, all nodes on a surface always experience the same shift in the direction of the surface normals. In contrast to the other types of boundary conditions unloaded side walls remain plane. Therefore, a clear determination of transverse strain is possible. In comparison to periodic boundary conditions it allows also a subsequent extension to several material sections for each deformation mode, but also involves additional restrictions.

For validation of the lateral material behaviour the uniaxial tension test is filmed with a high-speed camera. Afterwards, digital image correlation is used to extract the axial and the lateral stretch. This experiment is carried out on the foamed and the corresponding pore-free material.

Due to the inhomogeneous pore distribution uniaxial tension in different main directions lead to different stress responses if the sub-cell is not representative. Here, the variation are below 1% with stresses of 0.91 MPa (z-direction), 0.92 MPa (y-direction) and 0.95 MPa (x-direction) at 100% elongation. The simulation results reveal a softer response of the micromechanical modelling in comparison with the macromechanical approach, see Fig. 8.

The deviations are caused by a lower stiffness at strains below $\lambda = 1.4$. In comparison with the experiment the micromechanical approach underestimates the real behaviour whereas the macromechanical approach slightly overestimates it. Clearly, within the micromechanical sub-cell besides uniaxial tension further loading modes are eminent. The ideal uniaxial mode is assumed for the macro model.

Comparing the lateral behaviour, the micromechanical model predicts the experiment very well, see Fig. 9. At higher strains the macromechanical modelling approach diverges from the experiments. The deviations result from various reasons. The macromechanical model does not describe the full microstructure of the foam. Within the micromechanical approach fine, reinforcing structures like cell walls are overlooked by the segmentation. Light microscopic studies reveal that the thickness of overlooked cell walls is in the same order as big filler agglomerates. Such disorders evoke a local stress concentration. In both approaches they are neglected. In addition, we assume the pore-free material totally equals the matrix material within the foam. Due to the production process a small amount of free volume can occur leading to a porosity $\phi \neq 0$. Furhtermore, inner gas pressure within the pores has a small stiffening effect.

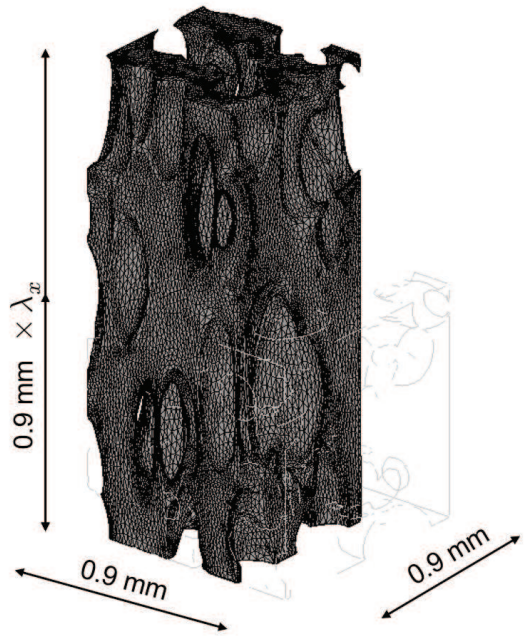

Figure 7: Uniaxial tension test on a sub-cell of the foamed elastomer

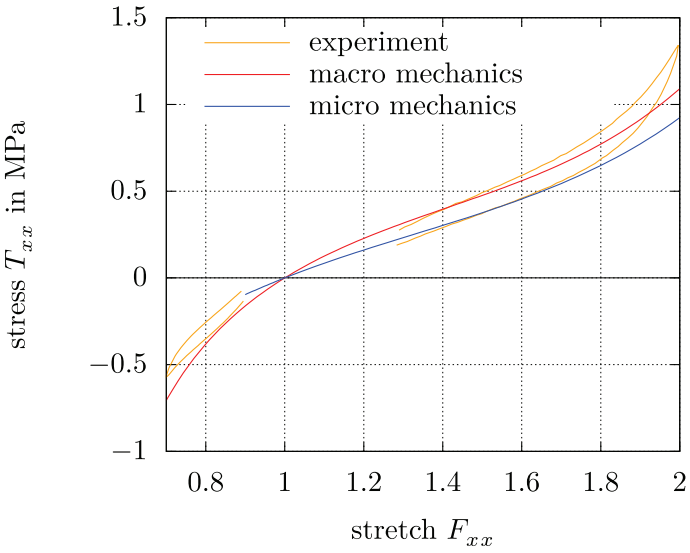

Figure 8: Comparison of the stress-strain behaviour between the micromechanical and the macromechanical modelling (1st Piola-Kirchhoff stress)

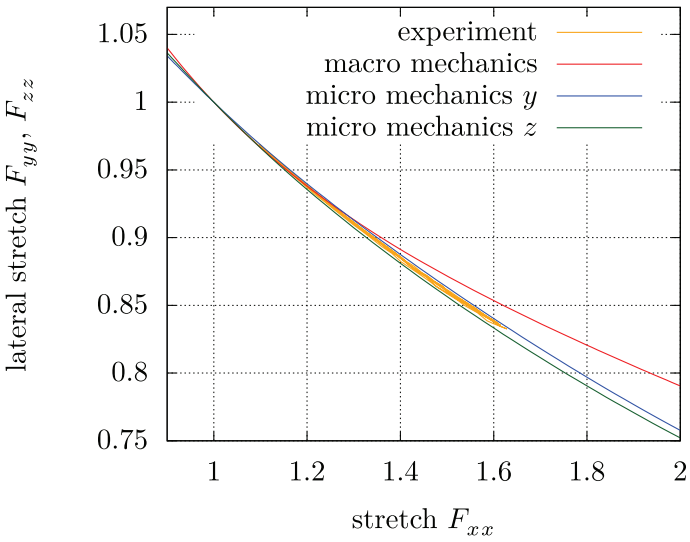

Figure 9: Comparison of the transverse contraction behaviour between the micromechanical (tension in x-direction) and the macro mechanic modelling. Due to the inhomogeneous pore distribution for the micromechanical simulation the two lateral directions are shown.

6 CONCLUSIONS

In principle, two approaches are conceivable for the modelling of cellular materials. The macromechanical modelling considers only the enveloping geometry of a component or test specimen. This allows an efficient implementation, but does not allow any consideration of the real pore structure. In contrast, the micromechanical modelling captures the local structures and their detailed deformations. For the macromechanical modelling the approach of Danielsson, Parks, & Boyce (2004) is extended to higher terms. The simple approach is based on the idealized idea of a pore as a hollow sphere, which is assigned an ideal incompressible, hyperelastic material model. Due to the higher order terms numerical integrations schemes are used to derived the strain energy function of the foamed material.

The efficient parameter identification via pore-free materials and density measurements of foamed and pore-fore material makes this modelling approach usable for industrial application like for simulation of car door seals. Although, the prediction of the lateral behaviour using the macromechanical approach lacks in accuracy, it can offer fast first results. By adjusting the porosity parameter for certain areas of a component, one can account for varying pore distributions within it. Micromechanical modelling offers a more accurate prediction and insights in the local loadings in the cell structure, but results also in high effort for measurement via CT, geometrical modelling and high computational costs. In principle, the micromechanical model reveals that a more accurate pore structure and higher non-linear effects stemming from the high local deformations of the matrix material of the foam has to be considered in a macromechanical approach.

Future works include the extension to more sophisticated models for elastomers, cf. Plagge, Ricker, & Klüppel (2019).

REFERENCES

ASTM Committee E02 on Terminology (Ed.) (2005). *Dictionary of Engineering Science & Technology* (10. Aufl. ed.). West Conshohocken: ASTM International.

Blatz, P. J. & W. L. Ko (1962). Application of Finite Elastic Theory to the Deformation of Rubbery Materials. *Transactions of the Society of Rheology 6*, 223–251.

Danielsson, M., D. M. Parks, & M. C. Boyce (2004). Constitutive modeling of porous hyperelastic materials. *Mechanics of Materials 36*(4), 347–358.

Diebels, S. (2000). *Mikropolare Zweiphasenmodelle: Formulierung auf Basis der Theorie poröser Medien*. Habilitationsschrift, Universität Stuttgart, Stuttgart.

Ehlers, W. & G. Eipper (1998). The simple tension problem at large volumetric strains computed from finite hyperelastic material laws. *Acta Mechanica 130*(1-2), 17–27.

Flory, P. J. (1961). Thermodynamic relations for high elastic materials. *Transactions of the Faraday Society 57*, 829–838.

Hill, R. (1978). Aspects of Invariance in Solid Mechanics. *Advances in Applied Mechanics 18*, 1–75.

James, A. G., A. Green, & Simpson G. M. (1975). Strain Energy Functions of Rubber: I. Characterization of Gum Vulcanizates. *Journal of Applied Polymer Science 19*(7), 2033–2058.

Jemiolo, S. & S. Turteltaub (2000). A Parametric Model for a Class of Foam-Like Isotropic Hyperelastic Materials. *Journal of Applied Mechanics 67*(2), 248–254.

Koprowski-Theiß, N. (2011). *Kompressible, viskoelastische Werkstoffe: Experimente, Modellierung und FE-Umsetzung*. Dissertation, Universität des Saarlandes, Saarbrücken.

Lebedev, V. I. (1976). Quadratures on a sphere. *USSR Computational Mathematics and Mathematical Physics 16*(2), 10–24.

Lewis, M. W. & P. Rangaswamy (2012). A stable hyperelastic model for foamed rubber. In S. Jerrams and N. Murphy (Eds.), *Constitutive Models for Rubber VII*, London, pp. 119–124. Taylor & Francis Group.

Matsuda, A., S. Oketani, Y. Kimura, & A. Nomoto (2017). Effect of microscopic structure on mechanical characteristics of foam rubber. In A. Lion and M. Johlitz (Eds.), *Constitutive Models for Rubber X*, London, pp. 575–579. Taylor & Francis Group.

MSC Software Corporation (2017). *Marc 2017 User Documentation: Volume A: Theory and User Information*. Newport Beach: MSC Software Corporation.

Ogden, R. W. (1972). Large deformation isotropic elasticity: on the correlation of theory and experiment for incompressible rubberlike solids. *Proceedings of the Royal Society of London A 326*, 565–584.

Plagge, J., A. Ricker, & M. Klüppel (2019). Efficient modeling of inelastic effects in filled rubber using load dependent relaxation times. In *Constitutive Models for Rubber XI: Proceedings of the European Conference on Constitutive Models for Rubbers XI (Nantes, France, 25-27 June 2019)*, Nantes, France.

Ricker, A. (2018). Experimentelle Untersuchungen und Erweiterung der kontinuumsmechanischen Modellierung von geschäumten Elastomeren. Master's thesis, Chemnitz University of Technology, Chemnitz.

Wang, H., W. Hu, & F. Zhao (2017). Numerical simulation of quasi-static compression on a complex rubber foam. *Acta Mechanica Solida Sinica 30*(3), 285–290.